Dissecting Star-forming regions with the GeMS MCAO instrument: lessons learned for optimal post-processing of WFAO data

Anaïs Bernard[a], Benoit Neichel[a], Thierry Fusco[a,b], Laurent Mugnier[b], Sophie Bounissou[a], Manash Samal[a], Morten Andersen[c], Annie Zavagno[a], and Henri Plana[d]

[a]Aix Marseille Université, CNRS, LAM (Laboratoire d'Astrophysique de Marseille) UMR 7326, 13388, Marseille, France
[b]ONERA (Office National d'Etudes et de Recherches Aérospatiales),B.P.72, F-92322 Chatillon, France
[c]Gemini Observatory, c/o AURA, Casilla 603, La Serena, Chile
[d]Laboratorio de Astrofísica Teórica e Observacional, Universidade Estadual de Santa Cruz, Rodovia Jorge Amado km16 45662-900 Ilhéus BA - Brazil

ABSTRACT

The advent of a new generation of Wide Field AO (WFAO) systems marks the beginning of a new era in high spatial resolution imaging. By using multiple Laser Guide Stars, WFAO significantly increases the field of view of the AO-corrected images, and the fraction of the sky that can benefit from such correction. The newly commissioned Gemini South Multi-Conjugate Adaptive Optics System (GeMS) combined with the infrared camera GSAOI is delivering almost diffraction-limited images over a field of ~ 2 arc-minutes across. In this paper, we first present recent observations of the young star-forming region N159W located in the Large Magellanic Cloud. We obtained deep JHKs images from the GeMS/GSAOI instrument and developed reduction tools, in order to photometrically study the properties of the stellar members of the cluster and to bring new elements to our understanding of the process of massive star formation. However, despite the excellent performance of the GeMS/GSAOI system, some variable residues are still limiting the correction quality over the field. In particular, GSAOI is severely affected by distortion that can strongly degrade the resolution when combining multiple frames and can consequently reduce the sensitivity. The accuracy of the distortion correction of an instrument is critical for its use for high- precision astrometry and photometry. In a second part of this paper, we investigate an optimal way to correct for the distortion following an inverse problem approach. The formalism as well as first simulation results are presented.

Keywords: Wide field adaptive optics, data processing, star forming region, photometry, correction of distortions

1. INTRODUCTION

By using multiple Laser Guide Stars (LGS), Wide Field Adaptive Optics (WFAO), consequentaly improve the performance of high spatial resolution imaging : The AO-corrected images Field of View (FoV) is increased as well as the fraction of the sky that can benefit from such correction. The Gemini Multi-Conjugated Adaptive Optics (MCAO) instrument GeMS is the first multi-Laser Guide Star operational system on sky. It has been implemented on the Gemini South telescope and commissionned in 2013. It works with two deformable mirrors conjugated at 0 and 9 km and a sodium-based LGS constellation composed of five spots : four are located at corners of a 60 arcsec square, with the fifth positioned in the center. GeMS, as a facility instrument, can direct its light output to different science instruments installed at the Cassegrain focus of the Gemini South telescope. Combined with the Gemini South Adaptive Optics Imager (GSAOI), it delivers near-diffraction limited images at Near-Infrared (NIR) wavelength (from 0.9 to 2.4 μm) over a FoV of $85'' \times 85''$. More details about the GeMS/GSAOI system and its commissioning results are described in detail in previous papers (see Neichel et al. (2013[1] and 2014[2]) , Rigaut et al. (2014),[3] D'Orgeville et al. (2012)[4] McGregor et al. (2004)[5] et Carrasco et al.(2011)[6]). However, despite the excellent performance of the GeMS/GSAOI system, the correction provided is not perfectly uniform

Further author information: (Send correspondence to Anaïs Bernard)
Anais Bernard: E-mail: anais.bernard@lam.fr
Benoit Neichel: E-mail: benoit.neichel@lam.fr

and may generate variable Point Spread Function (PSF) over the field. For instance, we observe in the data an average Full Width Half Maximum (FWHM) over the field ranged between 90 mas and and 145 mas depending on the filter and the natural seeing. The standard deviation associated is typically around 15 mas, corresponding to a variation of 10-15%. As well, the average Strehl Ratio (SR) range between 3% and 14% with a standard deviation from %1 to 3 % (see Tab.1). Those spatial variations of the PSF are present :

(i) on single frames, du to residuals from the AO correction ;

(ii) on stacked images, critically amplified by optical distortion generated by the system ;

Indeed, the optical components present in the instruments and the telescope as well as the camera GSAOI, introduce static and quasi-static distortions. They depend on environmental parameters like the LGS spot size or, the telescope pointing and may vary from one frame to another. Those dynamical distortions degrade the resolution and reduce the sensitivity by a factor two when combining multiple frames. From there, the ability to deal with the spatial variation of the PSF is critical for high-precision astrometry and photometry studies (see Massari et al. (2015),[7] Turri et al. (2015)[8]). Dedicated tools are needed on both axes : deal with the PSF variation over the field and properly correct for distortion. In a first part of this paper we expose upgrades implemented on the current photometric tool `StarFinder` to adapt it to variable PSF over the field of view. This analysis is done using simulated data as well as on sky data obtained with the GeMS/GSAOI system : a recent observations of a very active and young star-forming region N-159W located in the Large Magellanic Cloud (previously studied by Deharveng et al. (1992),[9] Testor et al. (2007),[10] Chen et al. (2010)[11]). We obtained deep J,H, and Ks images in order to study the properties of the cluster stellar members and bring new elements to our understanding of the massive star formation process. In a second part of this paper we present an existing distortion correction tool, its performance and limitation. We investigate then, an optimal way to correct for the distortion following an inverse problem approach based on the work presented in Gratadour et al. (A&A 2005)[12] on image re-centering, but generalized to all distortion modes. We present here the formalism and the first simulation results.

2. OBSERVATIONS AND DATA REDUCTION

2.1 Observations

The data used for the analysis were obtained during the night of December 8th 2014 as part of program GS-2014B-C-2 (P.I. B. Neichel). Images corrected for atmospheric distortions were obtained using the Gemini South Muti-Conjugate Adaptive Optics System (GeMS) and obtained with the Gemini South Adaptive Optics Imager (GSAOI). GSAOI focal plane is formed by a 2×2 mosaic of Hawaii- 2RG 2048×2048 pixel arrays with 3.0" wide gaps. Images are recorded in a 85" $\times$ 85" field of view with a plate scale of ~20 mas. Details of the observations are summarized in Table 1. Images were recorded through J, H, and $K_s$filters. Each observation consists of one science fields dithered randomly by a 5" rms shift to remove gaps between the detectors and a similar scheme for the sky frames taken 2.5′away from the science field. The averaged resolution over the field, measured as the FWHM of the stars on single-exposure frames, is reported in Table 1 as well as the natural seeing (measured at zenith). The averaged FWHM in $K_s$is 105 mas, while the averaged Strehl ratio (SR) is 14%. Those performance are slightly worst than those expected for the good seeing conditions, but there are consistent with observations at low elevation, as it is the case for the LMC. The coordinates of the center of the field are RA = $05^h39^m40^s$; DEC = -69°45′55″. We have adjusted the field in order to encompass what was previously observed by Testor et al. (2006)[10] who previously studied this region.

TABLE 1. Observation details. FWHMs, and SRs averaged over ~ 200 stars uniformly distributed over the field and for all the individual frames. The corresponding standard deviations are also given.

Date	Filter	Individual exposure time	Number of frames	<FWHM> (mas)	σ_{FWHM} (mas)	<SR> (%)	σ_{SR} (%)	Natural seeing (") (″@ 0.55μm)	PA (degree)
Dec 8^{th}	J	80s	17	145	15	3	1	0.55	320
2014	H	80s	14	100	20	9	2	0.60	320
	K_s	80s	17	105	15	14	3	0.55	320

2.2 Data reduction

Data reduction was done following the same procedure as in Neichel et al. (2015)[13] using home-made procedures developed in `Yorick` (Munro & Dubois 1995).[14] The different steps are :

(i) creation of a master flat image based on sky flat images taken durind twilight of the same night ;

(ii) creation of a master sky frame based on the dedicated sky images ;

(iii) correct the science frame from the master flat and the master sky, as well as for detector non-linearities and different gains between each detector.

The last step requires to apply an instrumental distortion correction that we detail in 4.2.
Following this procedure, each individual image has been reduced, and eventually combined by filter, to produce three long-exposure and three short-exposure reduced images. Figure 1 shows the final three-color image built from the GeMS/GSAOI data in J (blue), H (green), and Ks (red) bands.

FIGURE 1. N159W false three-color GeMS/GSAOI image combining J (blue), H (green), and K_s(red). North is up and east is left. The width of the image (East to West) is 90 arcs.

3. PHOTOMETRIC STUDY

3.1 Flux measurement with StarFinder

Flux measurement was done following a method using StarFinder (Diolaiti et al. (2000)[15]). As explained in Neichel et al. (2014a),[2] du to the complex structure of an AO PSF and its variation across the field and the frames, AO-photometry requires PSF-fitting algorithms which provide more accurate results than needed for regular aperture photometry. StarFinder does not use any model but it builds an empirical PSF by combining several stars in the image. In order to adapt this tool to a variable PSF over the filed, we divide the field in sub-fields, and study each sub-field individually. Of course, there is a trade-off between having enough stars per sub-fields, so that an accurate PSF model can be extracted, and keeping the sub-field as small as possible to keep the PSF variations effect to a minimum. In the case of N159W we experimented with different sub-field size. The minimum residual is obtained for sub-fields of size 16″× 16″, shifted by 8″(in x or y) in order to introduce overlap between the frames. Each star will then be measured several times, with different set of PSFs, which can be used latter as a photometric error estimation.

The StarFinder fine tuning present three critical parameters : the number of iterations, the relative threshold, and the correlation threshold for star extraction at each iteration. We adjusted those parameters so that every single faint star will be detected without too much contamination from the remaining bad or hot pixels or from structures in the background. Our three final reduced images (J, H, and K_s) have different characteristics in terms of noise and resolution, so this set of parameters has to be optimized for each filter. Those parameters are summarized in Table 2. In order to detect as much of the faint stars as possible, we worked on binned images, where each 4 pixels are averaged into one. This operation degrade the resolution by a factor 2 but enables the detection of low magnitude stars without biasing the flux measurement. Moreover, as the pixel size is 20 mas, and the average resolution on the image is on the order of 100 mas, there is strictly no loss of information. We also flag all the saturated stars defined assuming a minimum detector full well depth of 50000 e-, so that there are excluded from both the star extraction and photometry process. Only three very bright stars were saturated in filter H and Ks. We derive their flux using the Infra Red Survey Facility (IRSF) catalog. The final flux catalog contain 2185 stars in J, 4187 in H and 3912 in Ks.

TABLE 2. StarFinder parameters used for the star detection and photometry measurement, for each filter. The two values given for the threshold mean that the algorithm does two iterations, with a relative threshold at N sigma each.

Filter	Threshold	Correlation
J	[5, 2]	0.7
H	[5, 3]	0.7
K_s	[5, 4, 2]	0.75

3.2 Photometric error and completeness

As a performance criterion for the photometry study, we derive the completeness limit and the uncertainty magnitude for each filter. To determine the completeness of our images we used simulated stars embedded in the real images following the method described in Gennaro et al. (2011).[16] As for the photometric analysis, we divide the image in sub-field and use the corresponding local PSF computed by StarFinder to build the simulated stars. This method aims to reproduce the PSF variations in the field. Then, the fake stars are introduced at random positions on each subfields. One sets of 1000 fake stars is sufficient (see Neichel et al. (2015a)[13]). For each filters, we use a range of magnitude from 14.0 to 22.0, by steps of 0.5 mag. Once simulated stars are added to the images, we run the StarFinder detection again, using the exact same parameters as the ones used in 3.1. We then estimate the number of simulated stars that are properly detected and compute a completeness limit. At the same time, we can also estimate the photometric error by computing the standard deviation of the difference between the measured and simulated magnitudes. Results for the completeness limit are presented in Fig.2 . The values obtained, assuming 90% of completeness, are JHK_s limit = (21.55, 21.85, 21.1). This is respectively (2.55, 3.85, 4.5) magnitudes deeper than the limiting magnitude derived by the previous deeper observation of the region (Nakajima et al. (2005)[17]), see Bernard et al. in preparation. Results for the photometric uncertainties are presented in Fig.3. Those errors must be quadratically combined with the 0.1 mag. zero-point error. This gives the final photometric accuracy. The detectability of a source is depending on the local stellar density and the flux measurement settings used, but may also be affected by the diffuse background in the case of N159W. Thus, the simulations performed above can also be used to study the spatial distribution of the limit magnitude and photometric error across the field. The field is divided

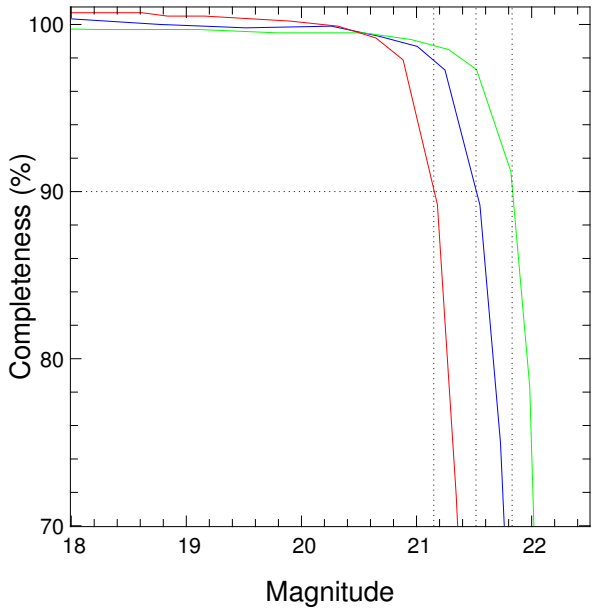

FIGURE 2. Completeness limit estimated from simulations

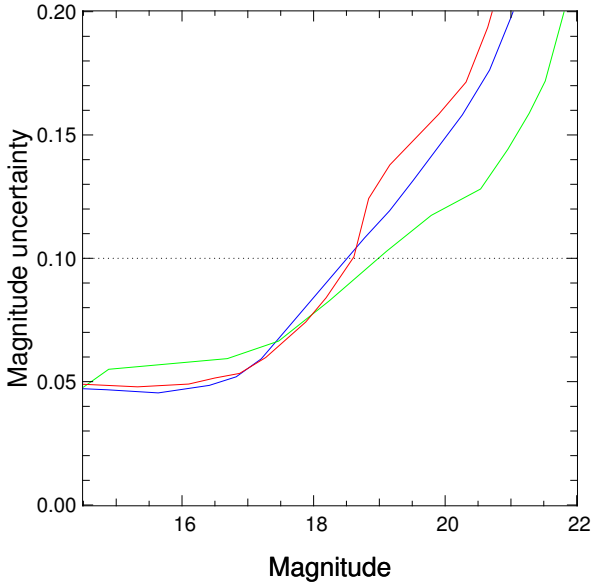

FIGURE 3. Photometric error estimated from simulations. Red is Ks, green is H, and J is blue.

into 32×32 sub-regions, in order to get a reasonable resolution. We still use 1000 simulated stars but compute 10 draws in order to improve the statistic in smaller sub-regions. For each region, we compute the average photometric error and the completeness level. This later is converted into limiting magnitude, using the same 90% detection criterion as above. Fig 4 displays the results for Ks filter. As expected, the lowest limit magnitudes are coinciding with the nebulous zone in the field. Note that only stars that have a magnitude uncertainty lower than 0.1 mag and a magnitude completeness higher than 90% are consider to be reliable for scientific analysis. For our specific case of N159W, it represents around 50% of the total star number. In order to improve the photometric and astrometric performance and increase the fraction of the stars that can be use for the analysis, we are addressing, in the next part, the key problem of the correction of the distortions.

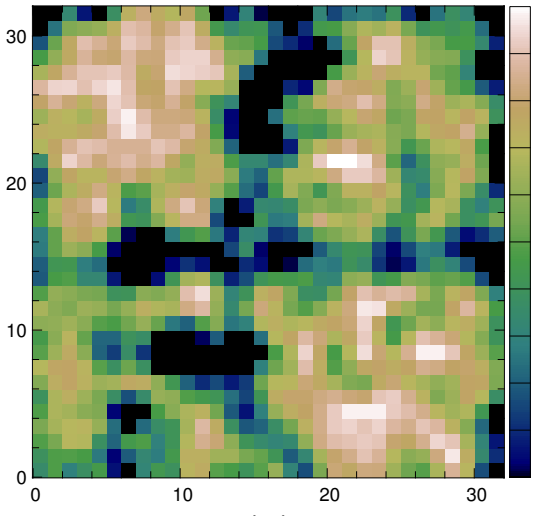

FIGURE 4. Spatial distribution of the completeness in Ks filter. Color scale is the limit magnitude (min is black ~ 20.5 mag and max is white ~ 21.3)

4. DISTORTION CORRECTION

4.1 Distortion caracterisation

The distortion in GeMS/GSAOI data are mostly coming from the off-axis parabola present in the AO bench. Those distortions have been estimated to be on the order of 0.5 ″(peak value). We expect them to mostly be low spatial orders. However, from the analysis carried in Neichel et al. (2014b),[18] it has been showed that higher spatial order are also present (around 15 degrees of freedom). Part of these high order distortions might be due to errors in the gaps correction. Indeed, the camera is composed of four distinct detectors separated by gaps. During the data reduction process, the four detectors are considered to be perfectly positioned, which might not be the case in reality. During the dithering of the telescope, if a star move from one detector to another between the different frames, this will introduce high order of distortion. Another source of errors comes from dynamical distortions, which depends on the NGS constellation and environmental factors like the telescope pointing and the dithering. In the next sections, we describe the current tools available to correct the images from distortion, and in a second part, we describe a new method of correction currently in development.

4.2 Existing tool

As mentionned above, the GeMS/GSAOI instrument is affected by static and quasi-static distortions. To deal with those distortions, we used a distortion map derived from GeMS/GSAOI observations of NGC 288 that we correlated with HST-ACS images. This distortion map leads to a residual star positioning accuracy of ∼0.2”. This is not good enough for the GeMS/GSAOI delivered image quality, which is typically around 80 mas. Moreover, this distortion calibration only accounts for the static instrumental distortions and the dynamical distortions still need to be compensated for. This dynamical distortions contribution has to be corrected frame by frame, taking one of them as the astrometric reference. By using high-order polynomials and the position of relatively bright stars common to all the frames we are able to cross-register the images together following these steps for each image :

(i) creation of a polynomial base $(P(x,y))_i$ of distortion modes type :
$P_i(x,y) = C_{i,0} + C_{i,1} + C_{i,2}y + C_{i,3}x^2 + C_{i,4}xy + C_{i,6}y^2 + \ldots$;

(ii) measurement of the vectors V_x and V_y of difference of position between the given image and the reference for each relatively bright stars common to all frames (mag < 21) ;

(iii) perform of a Levenberg–Marquardt fit of the V_x and V_y vectors on the polynomial base and determination of the α_i and β_i coefficients such that : $V_x = \sum \alpha_i P_i$ and $V_y = \sum \beta_i P_i$;

(iv) application of the inverse distortion map to the full image.

The N159W field is a ideal case that provide a large number of references, and by using 15 degrees of freedom per axis, we obtain a correction with a typical precision of 1 pixel corresponding to 20 mas. This method allows us to not degrade the quality of the images but is not precise enough for high-precision astrometry and photometry studies, especially on sparse fields. Indeed, the main limitation of this method is that it requires a large number of polynomial orders (15 degrees of freedom) to converge toward a minimal residual distortion (see Neichel et al. (2014b)[18]). This means that a large number of well isolated and bright stars are needed, which is not often the case. Another inconvenient lies in the fact that the correction is based on a reference chosen within the data and so, not free from distortions.

4.3 Toward an optimal distortion compensation

Aiming to overcome the limitations seen in Sec4.2, we now investigate an optimal way to correct for the distortion following an inverse problem approach based on the work developed by D. Gratadour and L. Mugnier. The original work of Gratadour et al. (2005),[12] was focusing on image re centering while here we generalize it to all distortion modes. The method is based on the minimisation of a criterion J define as :

$$J(X_j^{ref}, d_i, M_i) = \sum_{i=1}^{N_{im}} \sum_{j=1}^{N_{star}} w_{i,j} \left| X_{i,j}^{data} - M_i(X_j^{ref} + d_i) \right|^2 \quad (1)$$

With :

$X_{i,j}^{data} = \begin{pmatrix} x \\ y \end{pmatrix}_{i,j}^{data}$ position of star j in the single-exposure frame i

$X_j^{ref} = \begin{pmatrix} x \\ y \end{pmatrix}_j^{ref}$ theoretical distortion-free position of star j taken as reference

$d_i = \begin{pmatrix} \delta x \\ \delta y \end{pmatrix}_i$ shift between the image i and reference

$w_{i,j}$ = flux factor of star j in image i

M_i = transformation matrix between image i and the reference

Considering that the best estimation of the distortion-free position of the star is the one that minimize the criterion we can rewrite it :

$$J'(X_j^{ref}, d_i, M_i) = \sum_{i=1}^{N_{im}} \sum_{j=1}^{N_{star}} w_{i,j} \left| X_{i,j}^{data} - M_i \left(\left(\sum_{i=1}^{N_{im}} w_{i,j} M_i^T M_i \right)^{-1} \cdot \sum_{i=1}^{N_{im}} w_{i,j} M_i^T (X_{i,j}^{data} - M_i d_i) + d_i \right) \right|^2 \quad (2)$$

By deriving this expression we will be able to determine the different distortion parameters and the distortion-free position of the stars that minimize the criterion for each star in each image. Those estimated parameters would be the more probable ones, in a statistical way. This is a very general formalism that can apply to all distortion mode. In the next part, we describe the implementation of this method considering the three first mode of distortion that are : the two shift according the the x and y axis (mostly due to the dithering) and the scale factor. Note that to be consistent with physical phenomenon, the matrix transformation is applied to the shifted positions : indeed, following the photon path, the dithering is happening before the distortion introduced by the instrument.

4.4 Simulation results

As mentioned earlier, the implementation part has been done considering the three first mode of distortions : the two shift according the the x and y axis (respectively δ_x and δ_y), that include the dithering effect, and the scale factor (m). Thus, there will be, for each frame i, a triplet $[\delta_x, \delta_y, m]_i$ of distortion parameters associated to the this frame. In this particular case, the expression of the transformation matrix between the image i and the reference become :

$$M_i(m_i) = \begin{pmatrix} m_i & 0 \\ 0 & m_i \end{pmatrix} \quad \text{with m}_\text{i} \text{ the scale factor associated to the frame i}$$

In this section we use simulated images in order to evaluate this method ability to :

(i) estimate the distortion parameters ;

(ii) correct the distortion ;

4.4.1 The estimation of the distortion

In a first time, we introduce well-known distortions on fake images, in order to determine the precision with which the algorithm is able to estimate the distortion parameters. To do so we build one simulated image composed of nine noise-free PSF regularly distributed over the field. We use this image as the reference where the position of the nine PSFs are the distortion-free position of the stars X_j^{ref} with $1 < j < 9$. We then introduce a random triplet of distortion parameters $[\delta_x, \delta_y, m]_i$ on this image using 3 to build the $X_{i,j}^{data}$. The process is repeated several times to obtain a datacube of ten distortionned images ($1 < i < 10$). The positions of the PSFs $X_{i,j}^{data}$ ($1 < i < 10$ and $1 < j < 9$) on each frame are considered to be perfectly known in a first time.

$$X_{i,j}^{data} = M_i(X_j^{ref} + d_i) \quad (3)$$

Using those stars positions as input and after running the method, we found that both, the distortion parameters $[\delta_x, \delta_y, m]_i$ of each frame and the distortion-free position of each PSF X_j^{ref}, are evaluate with the numerical precision of 10^{-7} pixel.

However, when it comes to on-sky data, the PSFs position are not perfectly known and the measurements are contaminated with noise. In order to predict the behavior of the algorithm confronted to real data, we now build noisy measurements by adding a Gaussian noise on the measured positions of the PSFs $X_{i,j}^{data}$ previously used. We do this randomly using a growing noise (σ_{noise}=[0,0.05,0.1,0.2,0.5,1,2]). Once the noise added, the distortion parameters and the distortion-free positions of the PSFs are estimated following the same method as described above. We then repeat the process 100 times for one given σ_{noise} and derive an averaged error of estimation associated to that given σ_{noise}.

Fig.5 (a) shows the error on the distortion parameters δ_x (in red) and δ_y (in magenta) estimation. Fig.5 (b) shows the error on the distortion-free position of the PSFs estimation (in blue). In both case, the error represents the distance, in pixel, between the true value and the estimated value. It is quadratically averaged on the ten images and nine PSFs (respectively for the distortion parameters and the distortion-free position of the PSFs) and on the 100 noise values. The errors are plotted versus the root mean square of the noise added.

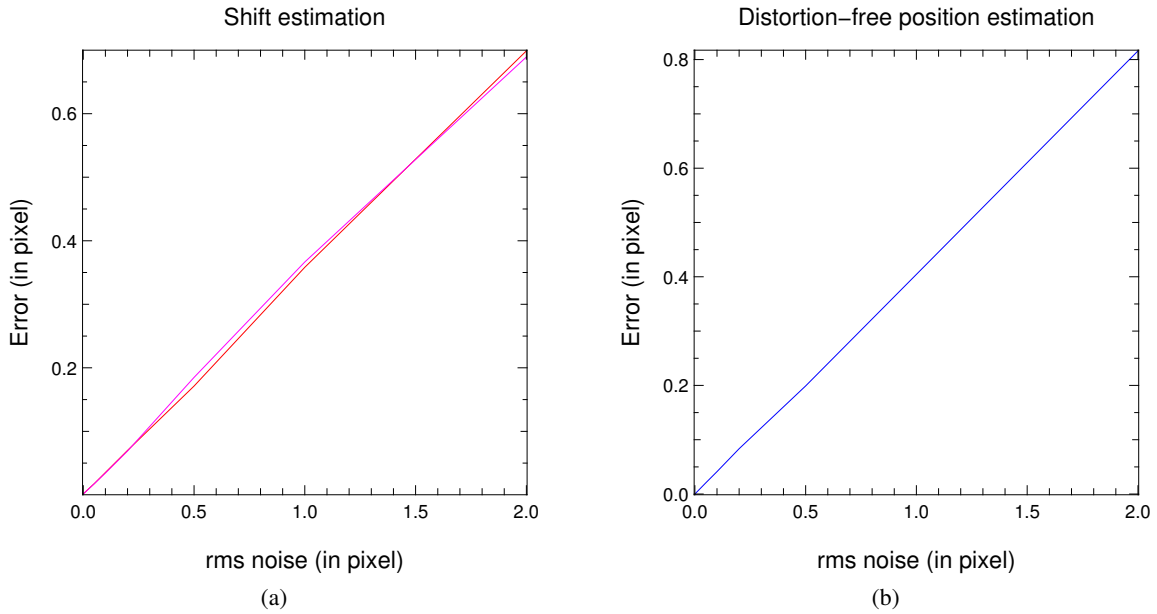

FIGURE 5. (a) show the error on the distortion parameters δ_x (in red) and δ_y (in magenta) estimation. (b) show the error on the distortion-free position of the PSFs estimation (in blue). In both case, the error represent the distance, in pixel, between the true value and the estimated value. It is quadratically averaged on the ten images et nine PSFs (respectively for the distortion parameters and the distortion-free position of the PSFs) and on the 100 noise values. The errors are plotted versus the root mean square of the noise added.

Note that a having a rms noise of 0.1 pixel on the measurement of a stars position on a typical set of GeMS/GSAOI data means dealing with a very faint object. For reference, a real data star fitted with a error of 0.1 pixel with a classical tool is shown in Fig. 6. This means that even working exclusively with very faint objects, barley detectable, we still reach a precision of 0.03 pixel (0.6 mas) on the estimation of the distortion, using the direct problem method. The method then seems particularly well adapted for sparse field, allowing the use of every detectable star in the field.

This means that using every detectable star in the field, even the faintest one,

4.4.2 Correction of the distortion

After estimating the distortion parameters and the distortion-free position of the PSF, we finally want to correct the different frames for it. To do so, we use the equation 4 derived from 3 :

$$X_{i,j,undist} = M_{i,estimated}^{-1} X_{i,j}^{data} - d_{i,estimated} \tag{4}$$

With $X_{i,j,undist}$ the position of the star j in the image i after applying the distortion correction.

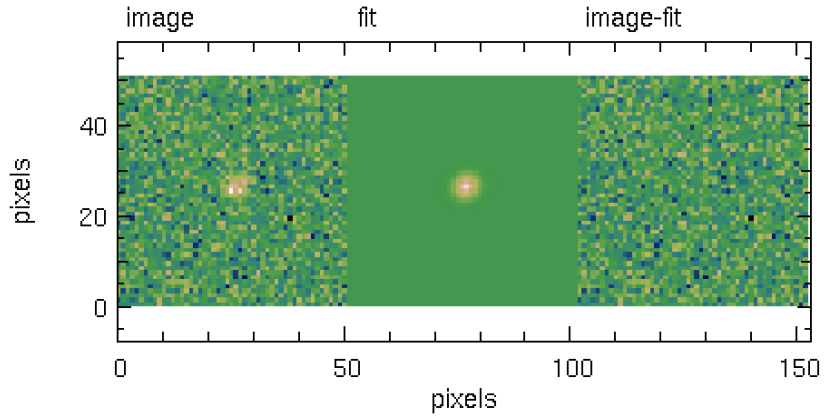

FIGURE 6. Example of a 0.1 pixel error fitted star from typical GeMS/GSAOI data. Example derived from the N159W data in Ks band.

In the absence of any noise, the correction is perfect and the corrected positions of the nine PSFs are identical for every frame : $X_{i,j,undist} = X_{j,undist} = X_j^{ref}$. But by introducing noise, the corrected position of one given PSF is variable from one frame to another. Thus, a good estimator of the correction efficiency is for one given PSF, the standard deviation (*std*) of this PSF position between the different frames. Besides, this criterion present the advantage to be directly linked to the stacked image quality. We introduce here the error of correction criterion , ϵ_n corresponding to the draw n :

$$\epsilon_n = \sqrt{\frac{1}{N_{PSF}} \left(\sum_{j=1}^{N_{PSF}} \underset{i}{std} \left(X_{i,j,undist} \right)^2 \right)} \tag{5}$$

In Fig. 7 are plot the ϵ criterion averaged quadratically on the 100 draws, following both, the existing method (black line) and the new method (red line), versus the *rms* noise introduced on the measures. Both are in pixel. The direct problem method appear to be more robust to the noise (black line) than the pre-existing method (red line). Plus, not to forget that the direct problem method allows an estimation of the distortion-free position of the stars whereas the existing tool use a non-distortion-free reference. Both are considerable advantages, in favor of the direct problem method.

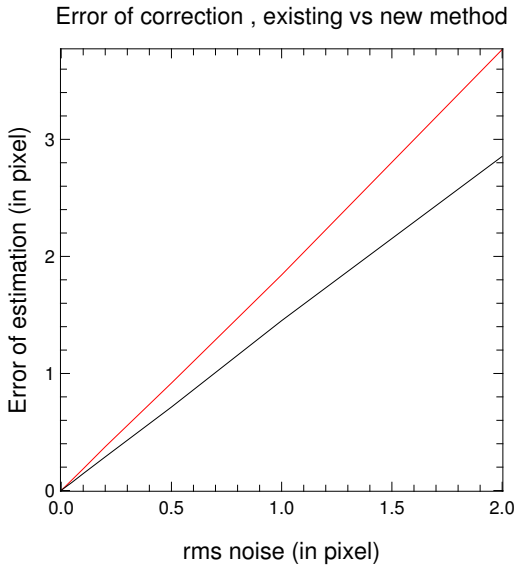

FIGURE 7. ϵ criterion following both, the existing method (red line) and the new method (black line), versus the *rms* of the noise introduced on the measures. Both are in pixel.

5. CONCLUSION

In this paper we have presented deep, high angular resolution, near-infrared images of the N159W star forming region located in the Large Magellanic Cloud. The data were obtained with the Near-Infrared Wide Field Adaptive Optic instrument GeMS/GSAOI recently implemented on the Gemini South telescope. Those images aim to explore the stellar content of the cluster and the massive star formation history of the region by doing a photometric study. Based on those real data, we evidence the limitation of the current reduction and analysis tools when it comes to Wide Field Adaptive Optics data. Indeed, despite the excellent performance of the adaptive optic correction, variable residuals are still limiting the quality of the image. Especially when combining multiple-frames, distortion effects consequently degrade the resolution and the sensitivity of the data. Thus, dedicated tools are needed to take into account those issues. In this article we address both aspects, dealing with spatial PSF variation and properly correcting from distortion. We presented in a first part, an alternative way to exploit the `StarFinder` code by considering sub-regions on the image to compute a local PSFs associated to one dedicated part of the field. We used this method to perform the scientific analysis of the N159W region (Bernard et al. in prep). In a second time, we presented a new method to correct from distortion that we are currently developing. This method is based on the least square minimisation of a criterion, as previously done by D. Gratadour et al. (2005)[12] for image re centering. We generalize here this method to al kind of distortion mode. Formalism as been presented as well as the implementation of a particular case in which we consider the three first mode of distortion : the shift according to the two axis and the scale factor. Based on first simulation results, we showed a strong robustness to the noise that allows the use of the faintest stars in the field to compute a reliable correction of the distortion. As the quality of the correction is proportional to the number of stars used to apply the correction, the robustness to the noise appear to be an essential parameter for sparse field astrometry and photometry. Moreover, this method presents the advantage to estimate a "distortion-free" position of the stars in the sky, while existing tools base the correction on a non distortion-free reference. The perspective of this work are the implementation of a complete version that will include the correction of any distortion mode, and, finally, the validation on real data.

ACKNOWLEDGMENTS

Based on observations obtained at the Gemini Observatory, which is operated by the Association of Universities for Research in Astronomy, Inc., under a cooperative agreement with the NSF on behalf of the Gemini partnership : the National Science Foundation (United States), the National Research Council (Canada), CONICYT (Chile), the Australian Research Council (Australia), Ministério da Ciência, Tecnologia e Inovação (Brazil) and Ministerio de Ciencia, Tecnologiaa e Innovación Productiva (Argentine).
The work was partly funded by the European Commission under FP7 Grant Agreement No. 312430 Optical Infrared Coordination Network for Astronomy and by the Office National d'Etudes et de Recherches Arospatiales (ONERA).
B. Neichel and A. Bernard acknowledge the financial support from the French ANR program WASABI to carry out this work.

REFERENCES

[1] Neichel, B., Vidal, F., Rigaut, F., Carrasco, E. R., Serio, A., Pessev, P., Winge, C., Dam, M. V., Araujo, C., Boccas, M., Fesquet, V., Galvez, R., Javier, L., Montes, V., Moreno, C., Rambold, W., Urrutia, C., and Vucina, T., "GeMS FIRST SCIENCE RESULTS," *AO4ELT Conference, 3rd edition* , 1–9 (2013).

[2] Neichel, B., Vidal, F., Dam, M. A. V., Garrel, V., Carrasco, E. R., Pessev, P., Winge, C., Boccas, M., Arriagada, G., Serio, A., Rambold, W. N., Javier, L., Moreno, C., Galvez, R. L., Montes, V., Vucina, T. B., Urrutia, C., Lopez, A., Diggs, S. J., Marchant, C., Ebbers, A. W., Trujillo, C., Bec, M., Trancho, G., Young, P. J., Colazo, F., and Edwards, M. L., "Gemini multi-conjugate adaptive optics system review II : Commissioning , operation and overall performance," *Monthly Notices of the Royal Astronomical Society* (December), 1–20 (2014).

[3] Rigaut, F., Neichel, B., Boccas, M., Dam, M. A. V., Arriagada, G., Fesquet, V., Galvez, L., Gausachs, G., Cavedoni, C., Ebbers, A. W., James, E., Javier, L., Montes, V., Perez, G., Rambold, N., Rojas, R., Walker, S., Bec, M., Trancho, G., Sheehan, M., Irarrazaval, B., Boyer, C., Ellerbroek, B. L., Flicker, R., Gratadour, D., Garcia-rissmann, A., and Daruich, F., "Gemini multi-conjugate adaptive optics system review I : Design , trade-offs and integration," *Monthly Notices of the Royal Astronomical Society* (December), 1–17 (2014).

[4] D'Orgeville, C., Diggs, S., Fesquet, V., Neichel, B., Rambold, W., Rigaut, F., Serio, A., Araya, C., Arriagada, G., Balladares, R., Bec, M., Boccas, M., Duran, C., Ebbers, A., Lopez, A., Marchant, C., Marin, E., Montes, V., Moreno, C., Petit Vega, E., Segura, C., Trancho, G., Trujillo, C., Urrutia, C., Veliz, P., and Vucina, T., "Gemini South multi-conjugate adaptive optics (GeMS) laser guide star facility on-sky performance results," *SPIE, Adaptive Optics Systems III* (January 2011), 84471Q–84471Q–21 (2012).

[5] McGregor, P., Hart, J., Stevanovic, D., Bloxham, G., Jones, D., Van Harmelen, J., Griesbach, J., Dawson, M., Young, P., and Jarnyk, M. A., "Gemini South Adaptive Optics Imager (GSAOI)," in [*Ground-based Instrumentation for Astronomy*], Moorwood, A. F. M. and Iye, M., eds., *Society of Photo-Optical Instrumentation Engineers (SPIE) Conference Series* **5492**, 1033–1044 (Sept. 2004).

[6] Carrasco, E. R., Edwards, M. L., Mcgregor, P. J., Peter, J., Doolan, M. C., Harmelen, J. V., Rigaut, F. J., Neichel, B., Artigau, E., Pessev, P., Colazo, F., Tigner, J., and Mauro, F., "Results from the commissioning of the Gemini South Adaptive Optics Imager (GSAOI) at Gemini South Observatory," *SPIE, Adaptive Optics Systems III* (2011).

[7] Massari, D., Fiorentino, G., McConnachie, A., Bono, G., Dall'Ora, M., Ferraro, I., Iannicola, G., Stetson, P. B., Turri, P., and Tolstoy, E., "GeMS MCAO observations of the Galactic globular cluster NGC 2808 : the absolute age," *Astronomy & Astrophysics* , 1–9 (2015).

[8] Turri, P., McConnachie, a. W., Stetson, P. B., Fiorentino, G., Andersen, D. R., Véran, J. P., and Bono, G., "Towards Precision Photometry with Extremely Large Telescopes : the Double Subgiant Branch of NGC 1851," *The Astronomical Journal* , 1–5 (2015).

[9] Deharveng_1992.pdf, "The stellar content of the LMC HII region N 59 A," *Astronomy & Astrophysics* **265**, 504–512 (1992).

[10] Testor, G., Lemaire, J. L., Kristensen, L. E., Field, D., and Diana, S., "VLT/NACO near-infrared imaging and spectroscopy of N159-5 in the LMC HII complex N159," *Astronomy and Astrophysics* **469**(2), 459–469 (2006).

[11] Chen, C. R., Indebetouw, R., Chu, Y.-h., Gruendl, R. A., Heitsch, F., Seale, J. P., Meixner, M., and Sewilo, M., "SPITZER view of young massives stars i n the LMC HII Complexes. II. N159," *The Astronomical Journal* **721**, 1206–1232 (2010).

[12] Gratadour, D., "Sub-pixel image registration with a maximum likelihood estimator," *Astronomy and Astrophysics* **365**(443), 357–365 (2005).

[13] Neichel, B., Samal, M. R., and Plana, H., "Deep near-infrared adaptive optics observations of a young embedded cluster at the adge of the RCW41 HII region," *Astronomy and Astrophysics* (25464), 27 (2015).

[14] Munro, D. H., "Using the Yorick interpreted language," *Comput. Phys.* **9**(6), 609–615 (1995).

[15] Diolaiti, E. and Bendinelli, O., "Starfinder : A code for crowded stellar fields analysis," *ASP Conference Series* **216** (2000).

[16] Gennaro, M., Brandner, W., Stolte, A., and Henning, T., "Mass segregation and elongation of the starburst cluster Westerlund 1," *Monthly Notices of the Royal Astronomical Society* **412**(4), 2469–2488 (2011).

[17] Nakajima, Y., Kato, D., Nagata, T., Tamura, M., Sato, S., Sugitani, K., Nagashima, C., Nagayama, T., Iwata, I., Ita, Y., Tanabe, T., Kurita, M., Nakaya, H., and Baba, D., "Near-Infrared Imaging Observations of the N159/N160 Complex in the Large Magellanic Cloud : Large Clusters of Herbig Ae/Be Stars and Sequential Cluster Formation," *The Astronomical Journal* **129**(2), 776–789 (2005).

[18] Neichel, B., Lu, J. R., Rigaut, F., Ammons, S. M., Carrasco, E. R., and Lassalle, E., "Astrometric performance of the Gemini multi-conjugate adaptive optics system in crowded fields," **16**(September), 1–16 (2014).